ACS APPLIED MATERIALS & INTERFACES

Research Article

www.acsami.org

# In Vitro Hemocompatibility and Toxic Mechanism of Graphene Oxide on Human Peripheral Blood T Lymphocytes and Serum Albumin

Zhijia Ding,[†,‡,§] Zhijun Zhang,[†] Hongwei Ma,[†] and Yanyan Chen*[,†]

[†]Key Laboratory for Nano-Bio Interface Research, Division of Nanobiomedicine, Suzhou Institute of Nano-Tech and Nano-Bionics, Chinese Academy of Sciences, Suzhou 215123, China

[‡]Institute of Biophysics, Chinese Academy of Sciences, Beijing 100101, China

[§]Graduate University of Chinese Academy of Sciences, Beijing 100039, China

Supporting Information

**ABSTRACT:** Graphene oxide (GO) has shown tremendous application potential as a biomedical material. However, its interactions with blood components are not yet well understood. In this work, we assess the toxicity of pristine GO (*p*-GO) and functionalized GO (GO-COOH and GO-PEI) to primary human peripheral blood T lymphocytes and human serum albumin (HSA), and also study the underlying toxic mechanism. Our results indicate that *p*-GO and GO-COOH have good biocompatibility to T lymphocytes at the concentration below 25 $\mu$g mL$^{-1}$, but notable cytotoxicity above 50 $\mu$g mL$^{-1}$. By contrast, GO-PEI exhibits significant toxicity even at 1.6 $\mu$g mL$^{-1}$. Further investigations show that although *p*-GO does not enter into the cell or damage the membrane, its presence leads to the increase in reactive oxygen species (ROS), moderate DNA damage, and T lymphocyte apoptosis. Interestingly, little effect on T lymphocyte immune response suppression is observed in this process despite *p*-GO inflicting cell apoptosis. The toxic mechanism is that *p*-GO interacts directly with the protein receptors to inhibit their ligand-binding ability, leading to ROS-dependent passive apoptosis through the B-cell lymphoma-2 (Bcl-2) pathway. Compared with *p*-GO, GO-COOH exhibits a similar toxic effect on T lymphocytes except keeping a normal ROS level. A proposed toxic mechanism is that GO-COOH inhibits protein receptor−ligand binding, and passes the passive apoptosis signal to nucleus DNA through a ROS-independent mechanism. On the other hand, GO-PEI shows severe hematotoxicity to T lymphocytes by inducing membrane damage. For plasma protein HSA, the binding of GO-COOH results in minimal conformational change and HSA's binding capacity to bilirubin remains unaffected, while the binding of *p*-GO and GO-PEI exhibits strong toxicity on HSA. These findings on the interactions of two-dimensional nanomaterials and biological systems, along with the enquiry of the mechanisms, would provide essential support for further safety evaluation of the biomedical applications of GO.

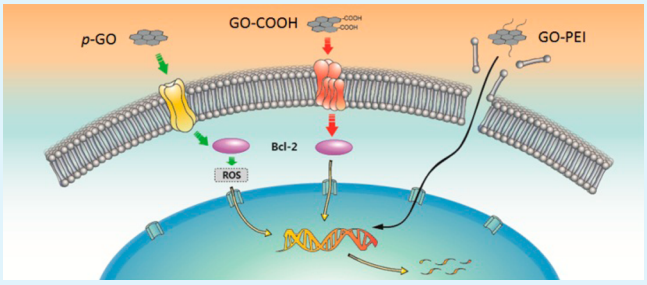


**KEYWORDS:** *hemocompatibility, graphene oxide, plasma proteins, T lymphocytes, toxic mechanism*

## 1. INTRODUCTION

Because of its interesting electrical, optical, mechanical, and chemical properties,[1] graphene oxide (GO) has found many potential biotechnological applications, including bioelectronics, biosensors, and biomedicine.[2−4] The tremendous attention attracted by the usage of GO in drug delivery systems,[5−13] cellular imaging,[5] and anticancer therapy[14−16] has spurred an interest in the interactions between GO and living systems. Much research has been performed to assess the in vivo and in vitro toxic effects of GO.[17−19] In vivo toxic studies indicate that GO has dominate accumulation in lungs[20−22] for long periods of time after being intravenously injected into rats or mice, which induces dose-dependent pulmonary toxicity and lung granuloma death.[20] For in vitro assessment of potential cytotoxic effects of GO, normal human lung cells (BEAS-2B),[23] human hepatocarcinoma cells (HepG2),[24] human breast MCF-7 cancer cells,[25] human umbilical vein endothelial cells (HUVEC),[26] human fibroblasts,[20,27] human lung cancer A549 cells,[28] HeLa cells,[29] etc., are used. Most of the studies reveal that GO exhibits dose- and time-dependent toxicity to human cell lines. However, cell lines may not be the optimal tool for biological research because they may contain an undefined set of mutations and chromosomal abnormalities that arise from multiple replications. Therefore, the toxicity results from cell lines may not comprehensively reflect GO's effect on human primary cells. Besides, because in most biomedical applications, intravenous injection is a common approach to administrate GO to living bodies, it is inevitable for GO to make contact with blood. This leads to the necessity for hemocompatibility studies of GO. Human blood is composed of blood cells (45% v/v) and blood

Received: July 31, 2014
Accepted: November 5, 2014
Published: November 5, 2014

  

plasma (55% v/v), and the latter is essentially an aqueous solution containing 92% water and 8% plasma proteins, so the interactions of GO with blood cells and plasma proteins are particularly important. However, there are few existing reports about the effects of GO on blood cells. Sasidharan et al.[30] reported that GO showed little hemolytic effect and insignificant levels of coagulation up to 75 $\mu$g mL$^{-1}$, but Liao et al.[27] proved GO had size-dependent red blood cell hemolytic activity. Singh et al.[31] showed that GO at 2 $\mu$g mL$^{-1}$ was thrombotoxic and amine-modified GO had absolutely no stimulatory effect[32] on human platelets. These apparent contradictions may be attributed to the influence of surface properties of GO with different morphologies and chemical compositions. Zhi et al.[33] demonstrated that GO increased the levels of three cytokines (TNF-$\alpha$, IL-1$\beta$ and IL-6) secreted by dendritic cells. However, to better understand GO nanomaterial's toxicity on the human body, further research of how GO interacts with other components within blood cells and plasma proteins is urgently needed.

In this work, we investigate the in vitro hemocompatibility and toxic mechanism of GO on human peripheral blood T lymphocytes and serum albumin. T lymphocytes, a type of white blood cell, play a central role in cell-mediated immunity. Most peripheral blood T lymphocytes are normally in non-proliferative resting phase ($G_0$ phase). Activation or induced deficiency of T lymphocytes may lead to chronic ailments like allergy, autoimmune diseases or cancer.[34] To our knowledge, there is little research of nanomaterial's toxic effect on $G_0$ phase T lymphocytes. Though Zhi et al.[33] reported that GO induced apoptosis of T lymphocytes, the T lymphocytes enriched by anti-CD3 magnetic beads are activated by anti-CD3 antibodies.[35] Therefore, in our study, primary human peripheral blood T lymphocytes (resting T lymphocytes, hereinafter referred to as T lymphocytes) are isolated and cultured with GO-based nanosheets to systematically evaluate the hemocompatibility of GO. Surface property of GO is taken as a variable because it is one of the key factors associated with nanomaterial's toxicity. Furthermore, the toxic mechanism of different GO is investigated in a toxicity profile in terms of its location in T lymphocytes, plasma membrane integrity, level of intracellular reactive oxygen species (ROS), DNA damages, cell apoptosis, as well as T lymphocytes immunological function. Also, the plasma proteins in culture medium exhibit strong interaction with GO and are coated on GO to mitigate the toxicity to T lymphocytes. To test whether GO's interactions with human plasma proteins would result in any adverse effects in terms of conformational and functional changes, human serum albumin (HSA) is chosen as a model protein because it is the most abundant protein in plasma, which plays a critical role in binding and transporting toxic metabolites.[36,37] On the basis of the above findings at cellular and protein levels, probable signaling pathways involved in GO toxicity are proposed.

## 2. EXPERIMENTAL SECTION

**2.1. Preparation and Functionalization of *p*-GO.** Pristine GO (*p*-GO) and functionalized GO (*f*-GO, containing GO-COOH, and GO-PEI) commonly used in drug delivery systems were chosen to assess the toxicity in primary T lymphocytes and HSA. Here, *p*-GO was prepared by Hummer's method[38] with minor modification. Briefly, native graphite flake (1 g) was mixed with concentrated $H_2SO_4$ (1.5 mL), $K_2S_2O_8$ (0.5 g, 1.85 mmol), and $P_2O_5$ (0.5 g, 3.52 mmol), and then incubated at 80 °C for 6 h to preoxidize the graphite. The product was then dried in air at ambient temperature overnight, after washing with deionized (DI) water until neutral and filtering. This preoxidized graphite was then subjected to oxidation by Hummer's method. The preoxidized graphite powder (1 g) was placed in concentrated $H_2SO_4$ (23 mL) at 0 °C. $KMnO_4$ (3 g) was added gradually by stirring while also keeping the temperature of the mixture below 20 °C. The mixture was then stirred at 35 °C for 2 h, followed by the addition of DI water (46 mL), and stirring was continued for 15 min. DI water (140 mL) was then added to terminate the reaction. Subsequently, 30% $H_2O_2$ (2 mL) was added and the color of the mixture changed to bright yellow. The mixture was centrifuged and washed with 10% HCl solution to remove residual metal ions. The precipitate was then washed with DI water and centrifuged repeatedly until the solution became neutral. To exfoliate the oxidized graphite, the product was treated with an ultrasonic probe at 400 W for 30 min, followed by centrifuging (Thermo, Heraeus Multifuge X1R) at 13 000 rpm for 30 min. The exfoliated GO was obtained in the supernatant. The precipitate was exfoliated repeatedly. *p*-GO obtained was steadily dispersed in DI water and would not precipitate for several months. GO-COOH was obtained through oxidization epoxy and hydroxyl groups on *p*-GO surface into carboxyl groups by chemical modification. Briefly, NaOH (5 g) and $ClCH_2COONa$ (5 g) were added to GO solution (1 mg mL$^{-1}$, 10 mL), followed by bath sonication for 2 h to convert the epoxy and hydroxyl groups into carboxyl groups. The resulting product was neutralized with diluted HCl and purified by repeated rinsing and centrifugation until GO-COOH was well-dispersed in DI water. GO-PEI was synthesized utilizing carboxyl activating regent (EDC) to initiate the formation of an amide linkage between *p*-GO and polyethylenimine (PEI, MW = 25 KD). PEI solution (10 mg mL$^{-1}$, 1 mL) and EDC solution (10 mg mL$^{-1}$, 5 mL) into *p*-GO solution (1 mg mL$^{-1}$, 10 mL). After applying ultrasonic vibration and stirring for about 10 min, we added additional EDC (10 mg mL$^{-1}$, 15 mL) and stirred overnight. GO-PEI was purified according to the following protocol: NaCl (1.6 g) was added to the mixture and dissolved. The supernatant was collected after centrifugation at 13 000 rpm for 2 h, and filtered via a 100 K ultrafilter. The retainer in the ultrafilter was repeatedly washed with aqueous solution containing 10% NaCl and 10% urea to remove any unreacted PEI. The product was repeatedly washed and then ultrafiltered to remove NaCl and urea, and was finally dispersed in DI water.

**2.2. T Lymphocyte Culture and Treatment.** Isolated T lymphocytes were maintained in RPMI 1640 culture medium supplemented with 10% FBS and incubated in a $CO_2$ incubator (Thermo, 3111) with a fully humidified atmosphere at 37 °C with 5% $CO_2$. Fresh isolated T lymphocytes were proven to keep viability within 24 h culture by Trypan blue staining experiments. Fresh isolated T lymphocytes ($1 \times 10^6$ mL$^{-1}$) were cultured in flasks and treated with different concentration of *p*-GO or *f*-GO for 24 h. No precipitate phenomenon occurred in the experiments. Cells were then centrifuged at 1000 rpm for 10 min. The supernatant was discarded and the cell pellet was resuspended in fresh medium. Samples of the T lymphocytes suspensions were used for the bioassays described below immediately.

**2.3. Transmission Electron Microscopic (TEM).** Ultrathin sections of the cells were analyzed using TEM to reveal the location of *p*-GO or *f*-GO in T lymphocytes. Briefly, after treated with 100 $\mu$g mL$^{-1}$ GO for 24 h, T lymphocytes were washed 3 times with PBS and then fixed in 2.5% glutaraldehyde for 2 h. Postfixation staining was done using 1% osmium tetroxide for 1 h at room temperature. Cells were washed and dehydrated in alcohol (40, 50, 70, 80, 90, 95, and 100% ethanol) and treated twice with propylene oxide for 30 min each, followed by treatment with propylene oxide, spurr's low viscosity resin (1:1), for 18 h. Cells were further treated with pure resin for 24 h and embedded in capsules containing pure resin. Resin blocks were hardened at 70 °C for 2 days. Ultrathin sections (70 nm) were cut using Reichert Jung Ultracut (EMUC6). The sections were stained with 1% lead citrate and 0.5% uranyl acetate and analyzed under a TEM (Tecnai G2 F20 S-Twin).

**2.4. WST-8 Cytotoxicity Assay.** WST-8 assay allows sensitive colorimetric determination of cell viability in cell proliferation and cytotoxicity. After respective incubation with various concentrations (0−100 $\mu$g mL$^{-1}$) of *p*-GO or *f*-GO for 24 h, cells were centrifuged at 1 000 rpm for 10 min and then resuspended in new culture medium to

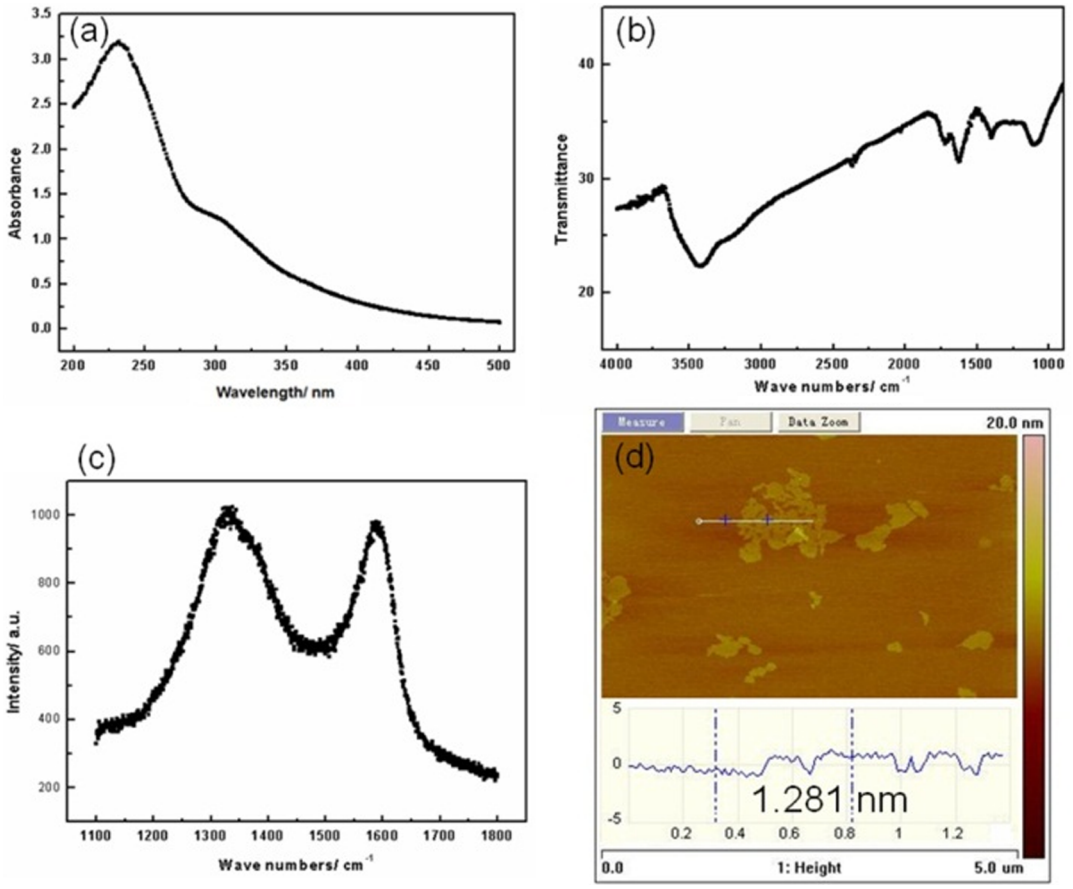


**Figure 1.** Characterizations of *p*-GO: (a) UV−vis spectrum, (b) FT-IR spectrum, (c) Raman spectrum, and (d) AFM height image of *p*-GO.

remove the GO. WST-8 solution (Beyotime) was added for another 4 h incubation. Absorbance was measured in a microplate spectrophotometer (PerkinElmer 2030) at 450 nm. The relative cell viability was calculated using eq 1

$$\text{cell viability (\%)} = \frac{\text{OD}_{\text{test}}}{\text{OD}_{\text{control}}} \cdot 100 \quad (1)$$

where $\text{OD}_{\text{test}}$ is the optical density of the cells exposed to GO and $\text{OD}_{\text{control}}$ is the optical density of the control sample.

**2.5. Lactate Dehydrogenase (LDH) Release Assay.** LDH leakage was used to evaluate the integrity of the plasma membrane of GO-treated cells. After respective incubation with *p*-GO or *f*-GO (100 $\mu$g mL$^{-1}$) for 24 h, the cell culture medium was collected for LDH measurement using LDH release assay kit (Beyotime). Absorbance was measured in a microplate spectrophotometer (PerkinElmer 2030) at 490 nm. Culture medium and LDH leakage reagent (Beyotime) were taken as the negative and positive control, respectively. The LDH leakage percentage was calculated using eq 2

$$\text{LDH leak (\%)} = \frac{\text{OD}_{\text{test}}}{\text{OD}_{\text{positive}}} \cdot 100 \quad (2)$$

where $\text{OD}_{\text{test}}$ is the optical density of the cells exposed to GO and $\text{OD}_{\text{positive}}$ is the optical density of the cells treated with LDH leakage reagent.

**2.6. DCFH-DA Assay.** Intracellular ROS generation was detected using 2,7-dichlorofl uorescein diacetate (DCFH-DA; Sigma, USA). Typically, cells treated with *p*-GO or *f*-GO (100 $\mu$g mL$^{-1}$) for 24 h were resuspended in culture medium containing 10 $\mu$M DCFH-DA for 30 min and intracellular ROS level was determined using a fluorescence microplate spectrophotometer (PerkinElmer 2030; excitation, 488 nm; emission, 525 nm). Culture medium and ROS positive control reagent Rosup (50 $\mu$g mL$^{-1}$) were taken as the negative and positive control, respectively. The ROS level was expressed as eq 3

$$\text{ROS level (\%)} = \frac{F_{\text{test}} - F_{\text{blank}}}{F_{\text{control}} - F_{\text{blank}}} \cdot 100 \quad (3)$$

where $F_{\text{test}}$ is the fluorescence intensity of the cells exposed to GO or the positive control, $F_{\text{control}}$ is the fluorescence intensity of the control cells and $F_{\text{blank}}$ is the fluorescence intensity of the wells without cells.

**2.7. Comet Assay.** Comet assay is a simple method for measuring DNA strand breaks in eukaryotic cells. After respective incubation with *p*-GO or *f*-GO (100 $\mu$g mL$^{-1}$) for 24 h, cells were washed twice and resuspended in PBS. A mixture of T lymphocytes and low melting-point agarose was added on microscope slides. Then the slides were immersed in cold lysis buffer and alkaline solution (pH > 13) each for 30 min and placed in a horizontal gel electrophoresis tank (LIUYI, DYCP-31DN) filled with fresh electrophoresis solution (300 mM NaOH, 1 mM EDTA). Electrophoresis was conducted at a low temperature for 30 min. After electrophoresis, the slides were rinsed with deionized water and immersed in 70% ethanol for 5 min, then drained and 50 $\mu$L of SYBR green I was added. Slides were scored with a fluorescence microscope (FLoid cell imaging station, Life technologies) and photographed. Culture medium and $H_2O_2$ (100 $\mu$g mL$^{-1}$) were taken as a negative control and positive control, respectively. At least 50 randomly selected images were analyzed for each sample. DNA damage was analyzed with the CASP software package. The percentage of DNA in the tail (% TailDNA) was used as the DNA damage indicator in our study.

**2.8. Annexin V-FITC/PI Assay.** Annexin V−fluorescein isothiocyanate (FITC)/ propidium iodide (PI) dual staining was employed to detect apoptotic and necrotic cells. After respective incubation with *p*-GO or *f*-GO (100 $\mu$g mL$^{-1}$) for 24 h, the cells were washed and stained with Annexin V and PI using Annexin V- FITC apoptosis detection kit (Beyotime). After incubation for 15 min, stained cells were resuspended in binding buffer (400 $\mu$L) and directly analyzed in flow cytometry

(FACSAria II, Becton, Dickinson Co.) by measuring the fluorescence at 530 and 575 nm.

**2.9. T lymphocyte transformation test (LTT) assay.** LTT assay was studied using T lymphocytes cultured in the presence of phytohemagglutinin (PHA) to evaluate the interferences of GO in T lymphocytes immune response. Typically, cells treated with *p*-GO or *f*-GO (100 $\mu$g mL$^{-1}$) for 24h were centrifuged at 1000 rpm for 10 min and then recultured in new RPMI 1640 culture medium containing PHA (100 $\mu$g mL$^{-1}$). After 68 h, WST-8 solution (Beyotime) was added for another 4 h incubation. Absorbance was measured in a microplate spectrophotometer (PerkinElmer 2030) at 450 nm. As positive and negative controls, T lymphocytes were also incubated in the presence of PHA and in the absence of PHA or GO, respectively. T lymphocytes immune response ability was calculated as eq 4

$$\text{immune ability (\%)} = \frac{\text{OD}_{\text{test}}}{\text{OD}_{\text{positive}}} \cdot 100 \quad (4)$$

where $\text{OD}_{\text{test}}$ is the optical density of T lymphocytes exposed to GO containing PHA, and $\text{OD}_{\text{positive}}$ is the optical density of T lymphocytes only treated with PHA.

**2.10. Western Blot Assay.** Western blot analysis was used to quantify the expression of Bcl-2 in T lymphocytes after 24 h treatment of GO. After respective incubation with *p*-GO or *f*-GO for 24 h, cells were washed twice in Tris-buffered saline, and 0.1 mL of RIPA buffer (Beyotime) containing freshly added protease inhibitors was added. Collected proteins were loaded on a 12% polyacrylamide gel, separated by gel electrophoresis, and transferred onto a PVDF membrane (Millipore, USA). The membranes were blocked and incubated with Rabbit monoclonal antibody directed against human Bcl-2 (Cell Signaling Technology), followed by HRP-conjugated secondary antibodies (Santa Cruz Biotechnology). The membranes were then reacted with ECL Western blot substrate kit (Beyotime) before exposure. $\beta$-tubulin was used as an internal control.

**2.11. Circular Dichroism (CD) Measurements.** CD spectra were recorded on a circular dichroism spectrometer model 410 (AVIV Biomedical Inc. Lakewood, NJ USA), over the range of 200−250 and 325−500 nm, using 0.2 and 1.0 cm cuvettes, respectively. The spectra were expressed as molar ellipticity [$\theta$] in deg cm$^2$ dmol$^{-1}$. The experiments were performed at 25 °C and three scans were averaged. For the conformational change detection, 100 $\mu$g mL$^{-1}$ HSA was mixed with 40 $\mu$g mL$^{-1}$ *p*-GO or *f*-GO for 2 h reaction. For the functional change detection, 100 $\mu$g mL$^{-1}$ GO was first mixed with 1 mg mL$^{-1}$ HSA for 2 h, after that 4.4 $\mu$g mL$^{-1}$ bilirubin (the molar ration of HSA bilirubin is 1:1) was added to each mixture for another 2 h. No precipitate phenomenon occurred in the experiments.

**2.12. Statistical Analysis.** Statistical analyses were expressed as the mean ± standard deviation of three independent experiments. The data were analyzed using student's t -test, in which statistical significance was calculated using untreated and GO-treated samples. * denotes $p < 0.05$ compared with untreated samples.

## 3. RESULTS AND DISCUSSION

**3.1. Characterization of GO.** *p*-GO prepared by Hummer's method is characterized by ultraviolet−visible spectroscopy (UV−vis), Fourier-transform infrared spectroscopy (FT-IR), Raman spectroscopy and atomic force microscopy (AFM). From the UV−vis spectrum in Figure 1a, *p*-GO shows a characteristic peak at near 230 nm, consistent with the literature report.[39] The D and G peaks in the Raman spectrum (Figure 1b) at 1325 and 1590 cm$^{-1}$ confirm the presence of *p*-GO. The peaks at 1720, 1640, and 1100 cm$^{-1}$ in FT-IR spectrum (Figure 1c) are characteristic of the C═O and C−O stretches of the ketone groups and epoxy groups on *p*-GO, respectively. The height of *p*-GO is about 1.28 nm, as shown in AFM image (Figure 1d), indicating that 1−2 layer *p*-GO is successfully prepared. Analysis of *f*-GO by UV−vis spectroscopy (see Figure S1 in the Supporting Information), FT-IR spectroscopy (see Figure S2 in the Supporting Information), zeta potential analyzer (see Figure S3 in the Supporting Information) and particle size analyzer (see Figure S4 in the Supporting Information) confirm successful functionalization of the products. The zeta potential data indicates that *p*-GO and GO-COOH are negatively charged at close potential level, whereas GO-PEI is positively charged.

**3.2. Effect of GO on Cell Viability.** The effect of GO on viability of T lymphocytes is determined after 24 h exposure to *p*-GO or *f*-GO at different concentrations (0−100 $\mu$g mL$^{-1}$) using WST-8 assay. The results in Figure 2 reveal that *p*-GO has

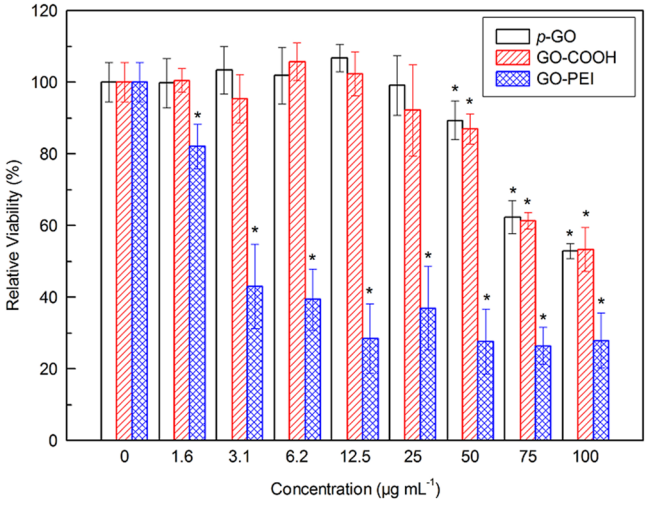


**Figure 2.** Cell viability of T lymphocytes incubated with GO at various concentrations for 24 h. * denotes $p < 0.05$ compared with the control.

negligible toxic effects below the concentration of 25 $\mu$g mL$^{-1}$. When increasing the concentration to 50 $\mu$g mL$^{-1}$, T lymphocytes start showing a reduction ($p < 0.05$) in cell viability. For *f*-GO, GO-COOH displays a similar dose-dependent toxicity relationship as *p*-GO, whereas GO-PEI treated samples shows a drastic decrease of viability with increasing concentrations of GO-PEI from 0 to 100 $\mu$g mL$^{-1}$, and these results suggest the significant toxic effect ($p < 0.05$) of GO-PEI even at 1.6 $\mu$g mL$^{-1}$. The significant toxicity of GO-PEI is due to the effect of PEI and graphene oxide, because the amount of conjugated PEI in GO-PEI is 42.9% based on element analysis. The detailed elucidation is shown in Figure S5 in the Supporting Information.

**3.3. Effect of GO on Cell Membrane and ROS.** To explore the toxic mechanism of GO, we incubated T lymphocytes with 100 $\mu$g mL$^{-1}$ GO for 24 h. We use TEM to locate GO in the treated T lymphocytes with the expectation that GO may accumulate at the cell membrane, be internalized to cytoplasm or travel into the nucleus after it makes contacts with T lymphocytes. The results (Figure 3a, b) show cell membrane integration of T lymphocytes treated by *p*-GO or GO-COOH. From the enlarged details in Figure 3d, e, some aggregates of *p*-GO or GO-COOH are found adsorbed on cell membrane and they could hardly be found inside cytoplasm or nucleus of T lymphocytes, indicating (1) the membrane is intact after binding of *p*-GO or GO-COOH and (2) no internalization of *p*-GO or GO-COOH to cytoplasm. Previous researches have reported the cellular uptake of GO depends on cell type. Yue et al. discovered only two phagocytes were capable of internalizing GO among six cell types (two macrophages and four nonphagocytic cells).[26] However, Mu et al.[40] in a study applying GO on nonphagocytic cells (mouse mesenchymal progenitor C2C12 cells) showed the

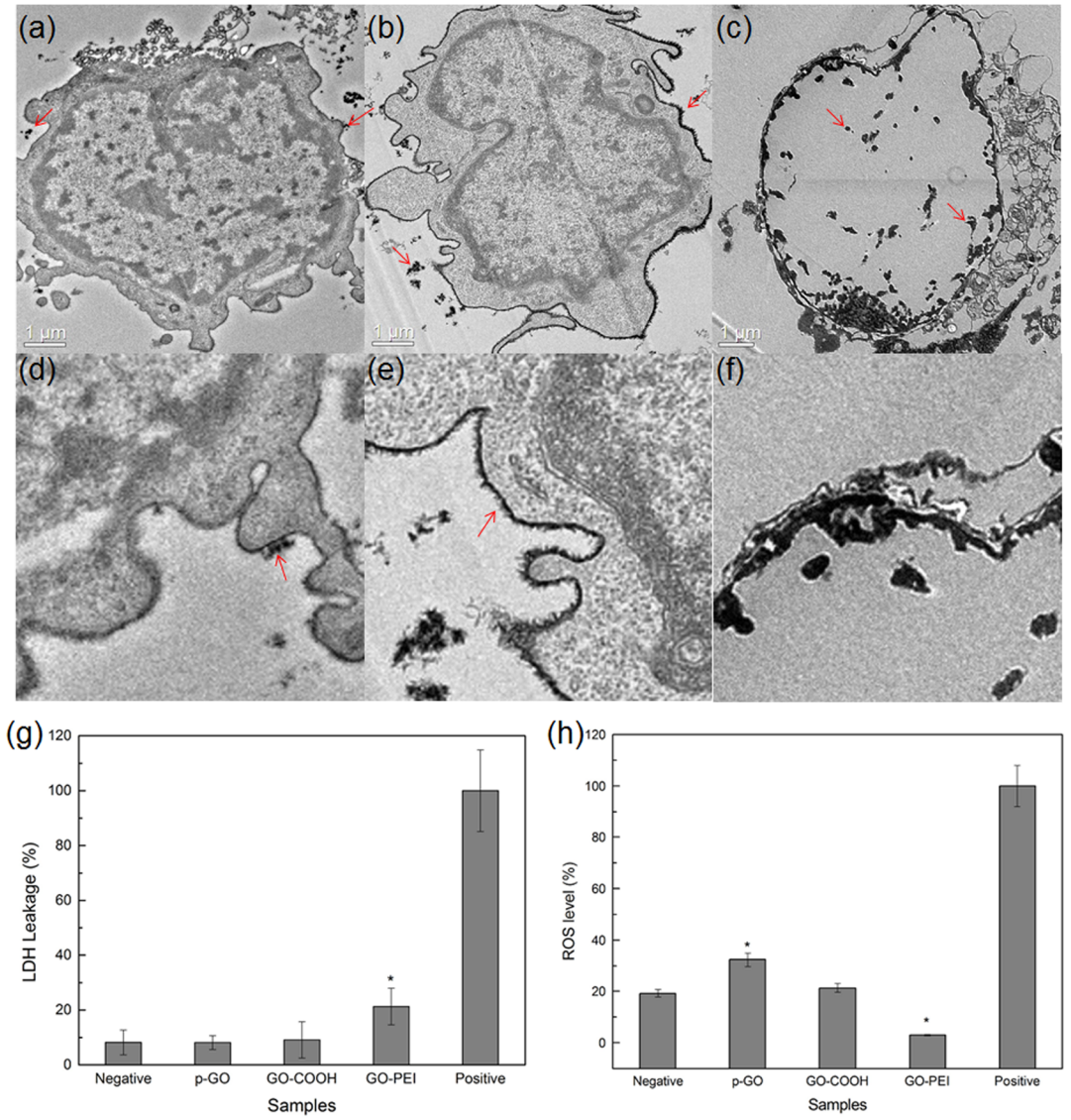


**Figure 3.** (a–c) TEM images of ultrathin sections of T lymphocytes treated with 100 $\mu$g mL$^{-1}$ GO. (a) *p*-GO, (b) GO-COOH, (c) GO-PEI. (d–f) Partial enlarged details of TEM images a–c, respectively. Red arrows indicate aggregated GO. (g) Plasma membrane integrity of T lymphocytes treated with GO (100 $\mu$g mL$^{-1}$) for 24 h using LDH leak assay and (h) oxidative stress responses of GO (100 $\mu$g mL$^{-1}$) in T lymphocytes using DCFH-DA assay. * denotes $p < 0.05$ compared with the negative control.

GO could be internalized via clathrin-mediated endocytosis. Although T lymphocytes are also nonphagocytic cells, the endocytic activity of G0 phase T lymphocytes is kept at a very low level,[41] thus no obvious *p*-GO or GO-COOH internalization occurs in our study. GO-PEI treated T lymphocytes show large hollow areas with the efflux of cytoplasm and endonuclear materials. The cell membrane is found to be discontinuous and the nucleus is occupied by GO-PEI (Figure 3c, f), which indicates that GO-PEI can transfer into the cell nucleus through membrane damage.

The findings of *p*-GO and GO-COOH absorption on cell membranes made us wonder whether they have interactions with the membrane proteins. Thus, we choose the T cell receptor (TCR), a common protein molecule on the membrane of T lymphocytes responsible for recognizing antigens, to investigate its binding with GO. The results in Figure S6 in the Supporting Information show that the fluorescence intensity of FITC conjugated anti-TCR on GO -treated T lymphocytes is weaker than that of the nontreated control, which means that both *p*-GO and *f*-GO interact with TCR and block the immunoreaction of TCR. This is a direct evidence of GO binding to the membrane protein. It could be inferred that such nonspecific binding of GO also occurs with other membrane proteins such as cytokines receptors (CKR), carrier proteins, ion channels, integrins etc.

Cell membrane damage through physical interaction with nanomaterials is a possible mechanism of toxicity.[42,43] The TEM images (Figure 3a-f) have exhibited the continuous membrane structures in *p*-GO or GO-COOH treated T lymphocytes. Furthermore, LDH release assay is used to confirm the membrane integrity of GO treated T lymphocytes. Figure 3g shows no significant LDH leakage from either *p*-GO or GO-COOH treated cells. This suggests that although *p*-GO and GO-COOH exerts toxicity at high concentrations, they do not induce physical damage to the plasma membrane. To GO-PEI treated T lymphocytes, cell membrane is damaged with 21.2% leakage of LDH compared to the positive control. This indicates that GO-PEI's interaction with the cell membrane causes significant physical damage to it, inducing cytotoxicity.

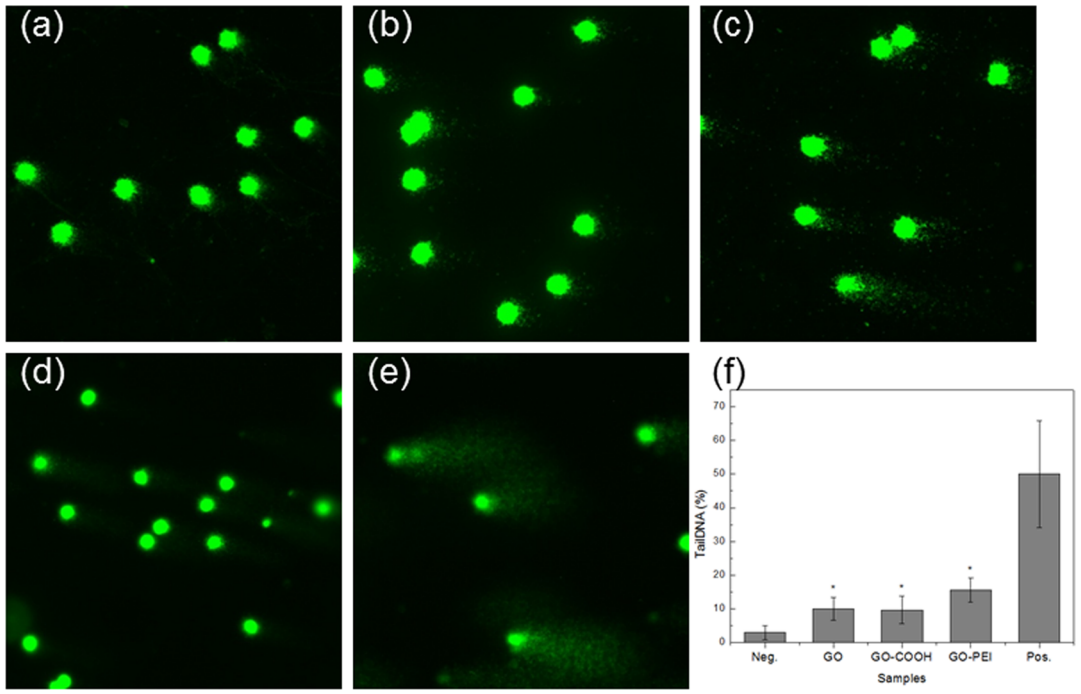


**Figure 4.** Single-cell gel electrophoresis results of T lymphocytes treated with GO (100 $\mu$g mL$^{-1}$) for 24 h using comet assay. (a–e) Photos of comet electrophoresis of T lymphocytes treated with (a) negative control, (b) *p*-GO, (c) GO-COOH, (d) GO-PEI, and (e) positive control. (f) summary of tail DNA percentage of T lymphocytes treated with GO for 24 h. * denotes $p < 0.05$ compared with the negative control.

No physical damage to the cell membrane by *p*-GO or GO-COOH supports the hypothesis that other mechanisms may contribute to their cytotoxicity. Oxidative stress has been proposed as one of the major toxic mechanisms of nanomaterials.[44] It is caused by increased ROS which can oxidize all biomolecules including DNA, lipids and proteins. Hence, the oxidative stress response of GO in T lymphocytes is studied using DCFH-DA assay. Figure 3h shows that *p*-GO treated T lymphocytes have a stronger fluorescence signal than the negative control, indicating an increased formation of intracellular ROS. GO-COOH-treated cells exhibit an insignificant fluorescence signal, suggesting normal intracellular ROS level compared to the negative control. GO-PEI-treated cells show a lower fluorescence signal, which is due to damage of the plasma membrane and the fluorescent product releases from the cell. So, the DCFH-DA assay results for GO-PEI-treated T lymphocytes are not reliable.

**3.4. DNA Damage, Apoptosis, and Immunotoxicity Induced by GO.** It is of great importance to investigate the genotoxicity of nanomaterials because there is a close correlation between DNA damage, mutation, and cancer.[45] Here, DNA damage of GO-treated T lymphocytes is detected using comet assay. The DNA damage is analyzed by CASP software and the percentage of DNA in the tail (%TailDNA) is used as DNA damage indicators. From Figure 4, we find *p*-GO and GO-COOH cause moderate DNA damage (9.9% and 9.7% tailDNA, respectively) compared to the negative control (2.9% tailDNA). GO-PEI induces grave DNA damage with a tailDNA of 15.6%.

A number of studies show that nanomaterials could induce apoptosis or necrosis. An apoptosis/necrosis assay on T lymphocytes treated with GO is performed using an Annexin V- FITC apoptosis detection kit. The results in Figure 5a–e show that, for *p*-GO-treated T lymphocytes, about 17.2% cells undergo early stage apoptosis (Q4) and 9.8% cells undergo late stage apoptosis (Q2). Zhi et al.[33] reported similar results that *p*-GO induced apoptosis of the activated T lymphocytes, but a more serious apoptosis occurred, with 67.4% T lymphocytes in late stage apoptosis being found in their work. It is because the activated T lymphocytes are more susceptible to apoptosis.[46] GO-COOH-treated T lymphocytes have similar apoptosis with *p*-GO that 18.3% cells are in early stage apoptosis and 9.5% in late stage apoptosis, whereas GO-PEI causes severe apoptosis with 76.8% cells in early stage apoptosis. This reveals that *p*-GO or GO-COOH induces moderate apoptosis while GO-PEI leads to severe cell apoptosis with only 4.8% healthy cells left (Q3). It is widely accepted that T lymphocytes apoptosis covers active and passive forms.[46,47] Passive apoptosis is strongly inhibited by antiapoptotic protein B-cell lymphoma-2 (Bcl-2). Active apoptosis requires TCR stimulation and involves death cytokines such as Fas ligand (FasL), which does not alter expression of Bcl-2. So the expression levels of Bcl-2 in GO-treated T lymphocytes can be used to distinguish these two apoptosis forms. From the results of Western blotting in Figure 5f, g, the level of Bcl-2 in *p*-GO and GO-COOH-treated T lymphocytes decrease by about 50% as compared to the control, indicating that *p*-GO and GO-COOH induce passive apoptosis through the Bcl-2 pathway. Also, we fail to detect the expression of FasL, which further confirms that *p*-GO or GO-COOH do not induce active apoptosis. Resting T lymphocytes rely on the interaction of TCR to survive. Growth cytokines are also reported to prevent passive apoptosis of T lymphocyte.[46] From the results in Figure S6 in the Supporting Information, GO is considered to interact with TCR as well as CKR and block them. So, the apoptosis induced by *p*-GO and GO-COOH is probably initialized by the inhibition of TCR and CKR to bind their ligands. For GO-PEI, the harvesting of proteins is difficult because of the destruction of the cell membrane with the efflux of cytoplasm, and thus the expression level of Bcl-2 in GO-PEI-treated T lymphocytes is not detectable.

It is interesting that *p*-GO induces apoptosis with a decrease in Bcl-2 and increase in ROS, whereas GO-COOH induces

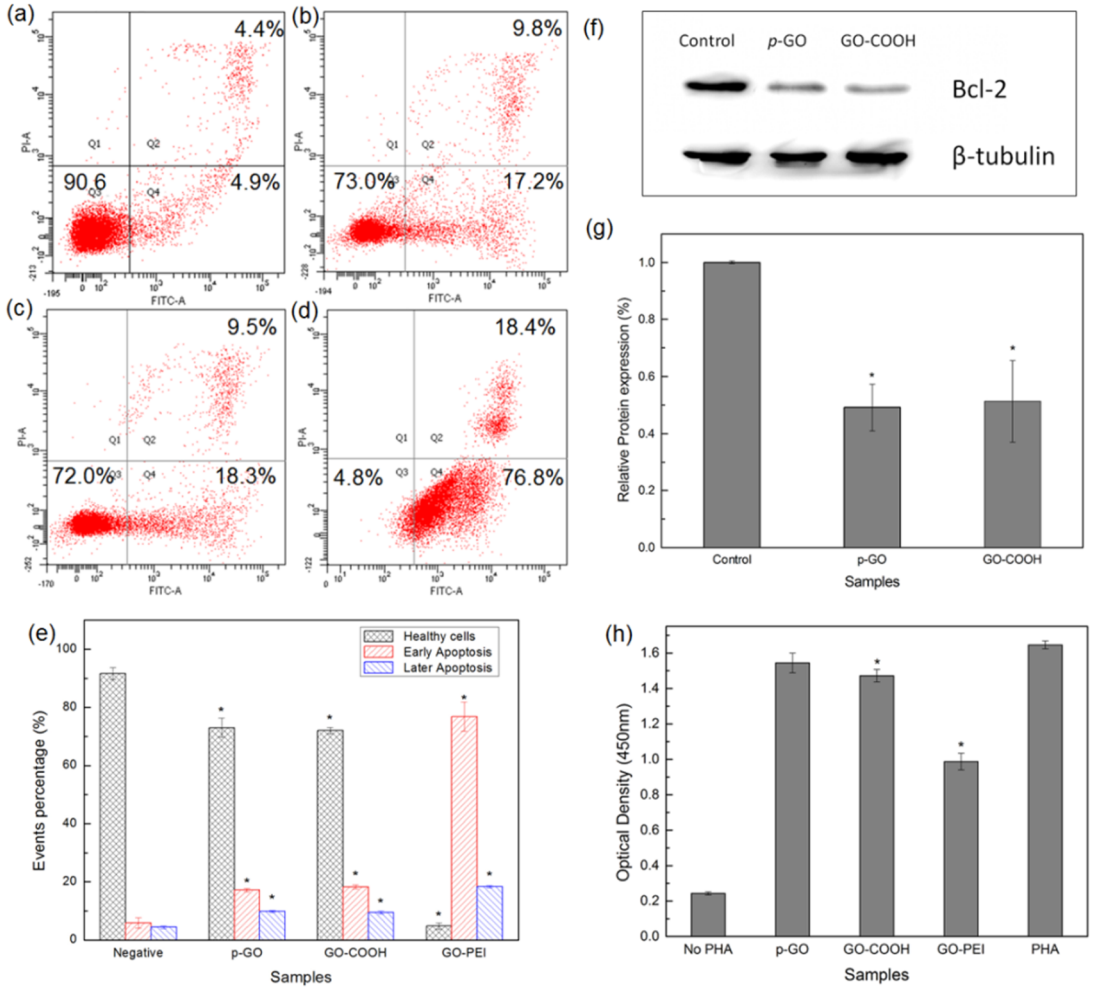


**Figure 5.** Apoptosis and immune response analysis of T lymphocytes treated with GO (100 $\mu$g mL$^{-1}$) for 24 h. (a–d) Scatter diagrams of T lymphocytes treated with (a) negative control, (b) *p*-GO, (c) GO-COOH, (d) GO-PEI using Annexin V-FITC and PI assay. (e) Summary of the apoptosis rate of T lymphocytes treated with GO for 24 h. * denotes $p < 0.05$ compared with the negative control. (f) Western blot analysis of Bcl-2 protein expression in T lymphocytes treated with GO. (g) Relative optical densities of Bcl-2 bands shown in f, * denotes $p < 0.05$ compared with the control. (h) Cell viability of T lymphocytes proliferation stimulated by PHA after exposed to GO. * denotes $p < 0.05$ compared with PHA-treated T lymphocytes sample.

apoptosis with a decrease in Bcl-2 while ROS is not involved. It has been suggested that cell apoptosis commonly involves the generation of ROS and that Bcl-2 protects against apoptosis by inhibiting the generation or action of ROS.[48,49] However, Jacobson et al.[50,51] suggested that ROS is not required for apoptosis and Bcl-2 protects against apoptosis in ways not dependent on the inhibition of ROS production. Ko et al.[52] also found myricetin induced ROS-independent apoptosis of HL-60 cells with a decrease of Bcl-2 protein. Furthermore, Bcl-2 is not only an antioxidant to inhibit the generation of ROS, but also associated with the calcium concentration within the lumen of the endoplasmic reticulum and protects against calcium mediated apoptosis.[53] Bcl-2 can even act as anchored proteins to form a heterodimers with proapoptotic protein Bax to regulate cell apoptosis.[54] The detailed apoptosis signal transduction mechanism induced by GO-COOH needs further research.

T lymphocytes play a major role in the immune response, and the interaction with GO may cause their stimulation or suppression. Upon activation of T lymphocytes by a foreign material, clonal proliferation of the cells takes place as part of the immune response. From the result of Figure 2, *p*-GO, GO-COOH, or GO-PEI does not increase the cell viability of T lymphocytes at either low or high concentrations. This indicates that GO could not trigger T lymphocytes proliferation. Immunosuppression by nanomaterials is another major concern due to the possible cytotoxicity to immune cells. LTT assay is applied to detect the proliferation of T lymphocytes to evaluate whether GO interferes with the normal immune response ability.[55] The WST-8 assay results in Figure 5h show that *p*-GO and GO-COOH cause tiny decrease of T lymphocytes immune response ability (93.8 and 89.4% remained), whereas GO-PEI strongly suppresses the immune response ability (60% remained). Interestingly, although *p*-GO and GO-COOH induce a significant decrease in cell viability and apoptosis, their influences on T lymphocytes immune response suppression are small. It is reported that resting T lymphocytes make response to PHA with the production of IL-2. IL-2 not only induces proliferation of T lymphocytes, but also causes the greatest susceptibility to active apoptosis. The feedback response of IL-2 is executed to balance the level of T lymphocytes through varying amounts of T cell proliferation and apoptosis.[46] Thus, *p*-GO and GO-COOH show little effect on T lymphocytes immune response suppression, though they induce apoptosis.

**3.5. Influence of Surface Property and Signaling Pathway.** Our results demonstrate that *p*-GO and GO-COOH exhibit similar biocompatibility on T lymphocytes, but

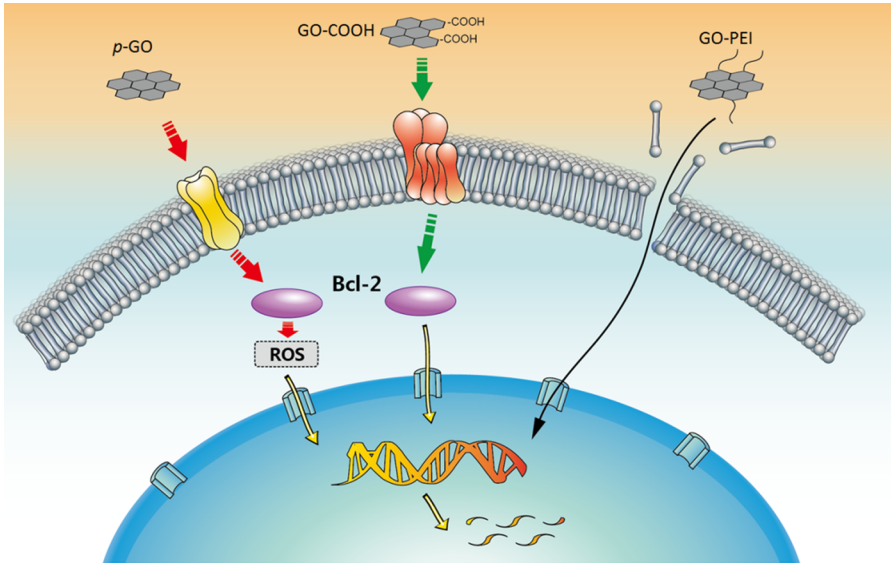


**Figure 6.** Schematic diagram showing proposed toxic mechanisms of GO on T lymphocytes based on the current data. From left to right are *p*-GO, GO-COOH, and GO-PEI, respectively. Dotted line indicates signal pathway and full line indicates the way of GO-PEI transport.

**Table 1. Hemocompatibility Analysis of GO on T Lymphocytes and HSA**

| | interactions with T lymphocytes | | | | | | | | interactions with HSA | |
|---|---|---|---|---|---|---|---|---|---|---|
| | location of GO | cell viability (%) | LDH leak (%) | ROS level (%) | early apoptosis (%) | tail DNA (%) | Bcl-2 expression (%) | immune ability (%) | $\alpha$-helix (%) | BBC (%) |
| control | | 100 | 8.2 ± 4.5 | 19.2 ± 1.5 | 4.9 ± 1.8 | 2.9 ± 2.0 | 100 | 100 | 61.5 ± 0.6 | 100 |
| *p*-GO | membrane | 52.8 ± 2.1[a] | 8.4 ± 2.5 | 32.3 ± 2.6[a] | 17.2 ± 0.6[a] | 10.0 ± 3.4[a] | 49.1 ± 8.3[a] | 93.8 ± 3.4 | 48.6 ± 0.6[a] | 34.7 ± 6.1[a] |
| GO-COOH | membrane | 53.3 ± 6.1[a] | 9.1 ± 5.6 | 21.3 ± 1.7 | 18.3 ± 0.7[a] | 9.7 ± 4.1[a] | 51.3 ± 14.3[a] | 89.4 ± 2.1[a] | 55.7 ± 0.9[a] | 96.3 ± 8.2 |
| GO-PEI | nucleus | 27.9 ± 7.7[a] | 21.3 ± 6.7[a] | 3.0 ± 0.2[a] | 76.8 ± 5.0[a] | 15.6 ± 3.5[a] | / | 60.0 ± 2.9[a] | 23.8 ± 2.9[a] | 4.9 ± 0.6[a] |

[a]denotes $p < 0.05$ compared with the control.

GO-PEI shows severe hematotoxicity to T lymphocytes by inducing membrane damage. One possible reason is the difference of the surface charge of GO: that *p*-GO and GO-COOH are negatively charged with close zeta potential while GO-PEI is positively charged. This result is consistent with the previous reports that positively charged particles are more toxic to cells than negatively charged particles.[56,57] The reason is that positively charged particles might show strong electrostatic adsorption with the cell membrane, which can enhance cell uptake and break the charge balance of the cell membrane or damage it. By contrast, the negatively charged particles show electrostatic repulsion to cell membrane, which results in the absence of cell uptake. Besides, *p*-GO induces increased intracellular ROS production but GO-COOH does not. This proves that carboxyl modification is an effective method to inhibit intracellular ROS generation.

Through the above systematic analysis, we demonstrate that *p*-GO adsorbs on the cell membrane without membrane damage or internalization, but it causes intranuclear DNA fracture and cell apoptosis. Also *p*-GO is found to bind membrane proteins such as TCR. A possible toxic mechanism (Figure 6) is that *p*-GO interacts directly with membrane protein receptors (such as TCR and CKR) and inhibits their normal ligands binding. Then, passive apoptosis signal is produced to cause DNA fracture with the decrease of Bcl-2, and ROS is also involved in the apoptosis mechanism. GO-COOH also inhibits the binding of membrane protein receptors with ligands and passes the apoptosis signal to nucleus DNA. However, the maintaining of normal ROS levels indicates GO-COOH leads to passive apoptosis through a ROS-independent signal transduction mechanism. GO-PEI causes significant physical damage to the plasma membrane, inducing cytotoxicity. All the hemocompatibility analysis data of GO on T lymphocytes are listed in Table 1.

**3.6. Effect of GO on Structure and Function of HSA.** In the toxicity study above, T lymphocytes are treated with different GO for 24 h and cultured in RPMI 1640 medium supplemented with 10% FBS. The FBS proteins in the supernatant of cell medium decrease (see Figure S7 in the Supporting Information) after adding *p*-GO, which suggests that *p*-GO has strong interaction with FBS proteins. The results in Figure S4 in the Supporting Information show that the hydrodynamic sizes of GO increase dramatically after incubation in culture medium. This further proves the interaction between GO and FBS proteins. For comparison, the viability of T lymphocytes treated with GO for 24 h in the RPMI 1640 medium without FBS is also studied. Apparently, cell viability of T lymphocytes cultured without FBS nutritional support is less than that with FBS. The two sets of WST-8 data (viabilities of T lymphocytes cultured with and without FBS) is normalized (viabilities of T lymphocytes in the absence of GO are used for each set's reference standard, respectively) to eliminate the influence of nutrition. The results in Figure S8 in the Supporting Information suggest that the cytotoxicity of GO to T lymphocytes is greatly mitigated at the presence of FBS, consistent with the results by Hu et al.[58]

It can be deduced from the results above that proteins have strong interaction with GO. In order to determine the effects of GO on plasma proteins, greater details are required. HSA, the

most abundant protein in plasma, is used as a model protein to study the interaction of GO with plasma proteins in terms of conformational and functional changes. CD analysis[59,60] is used to quantify the conformational changes of HSA induced by GO. It reveals two negative bands in the ultraviolet region at 208 and 222 nm, which are characteristic of an $\alpha$-helical structure, as HSA structure is predominantly $\alpha$-helical (approximately 67%). The

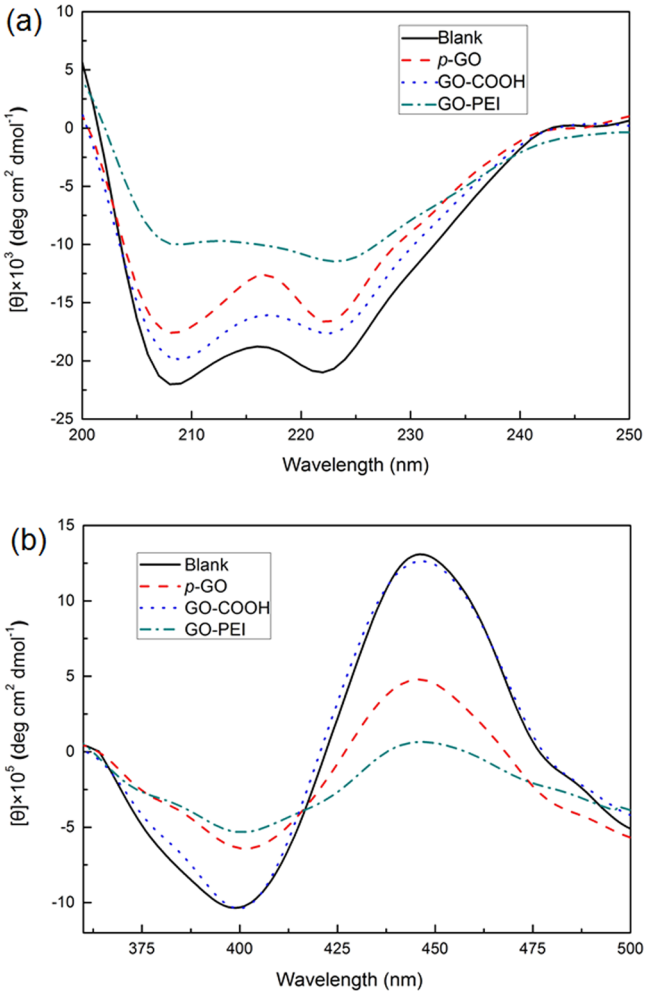


**Figure 7.** Effect of GO on HSA. (a) Effect of GO on HSA secondary structure determined by circular dichroism spectra. (b) Effect of GO on HSA function determined by Cotton effect of the bilirubin binding to GO-associated HSA.

CD spectra of HSA in the presence of GO are shown in Figure 7a. The $\alpha$-helix content is calculated based on eqs 5 and 6.[60]

$$\alpha\text{-helix}\ (\%) = \frac{-\mathrm{MRE}_{208} - 4000}{33000 - 4000} \cdot 100 \tag{5}$$

$$\mathrm{MRE}_{208} = \frac{\theta M}{10CLN_r} \tag{6}$$

where $\theta$ is the ellipticity value of the sample, $M$ is the molecular weight (Da) of HSA, $C$ is the HSA concentration (mg mL$^{-1}$), $L$ is the sample cell path length (cm), and $N_r$ is the number of amino residues. A decline in the $\alpha$-helix content of HSA is found after association with GO (Table 1). This means GO has an adverse effect on HSA conformation, and the magnitude of such adverse effect is ranked as GO-PEI > $p$-GO > GO-COOH.

Bilirubin is a toxic metabolite of heme. The binding of HSA and bilirubin prevents bilirubin encephalopathy from high bilirubin blood concentration. In this work, bilirubin binding to GO-associated HSA is investigated to verify the functional change of HSA influenced by GO. Normally, the Cotton effect curve is used to determine the bilirubin-HSA complex in the visible region by CD measurement and the amplitude is in proportion to the complex amount.[37] In our experiment, the Cotton effect curves of bilirubin binding to different GO-associated HSA and native HSA are measured, and the results are shown in Figure 7b. To quantify the functional change of HSA influenced by GO, the bilirubin binding capacity (BBC) of HSA associated with GO is calculated by eq 7.

$$\mathrm{BBC}(\%) = \frac{\theta_{\mathrm{peak,GO}}}{\theta_{\mathrm{peak}}} \cdot 100 \tag{7}$$

where $\theta_{\mathrm{peak}}$ is the peak ellipticity value of bilirubin-native HSA complex and $\theta_{\mathrm{peak,GO}}$ is that of bilirubin-GO associated HSA complex. The results demonstrate that BBC of HSA is clearly reduced after association with GOs except GO-COOH (Table 1). This suggests that $p$-GO and GO-PEI have adverse impacts on HSA function of bilirubin binding, whereas GO-COOH could interact with HSA without disrupting its function. The ranking of the adverse effect of GO on HSA function is GO-PEI > $p$-GO > GO-COOH. Also, the tendency of GO effect on HSA functional changes is in accordance with that on HSA conformational changes.

## 4. CONCLUSIONS

GO family nanomaterials have been widely used in biomedicine and have brought tremendous attention of their toxicity. The hemocompatibility study of GO based on the investigations at the cellular and protein levels are performed in this study. For T lymphocytes, this study demonstrates that $p$-GO has a dose-dependent cytotoxicity and exhibits no cytotoxicity at low concentration below 25 $\mu$g mL$^{-1}$. It is consistent with most toxicity analysis in other cell types.[20,27,28] Unexpectedly, our results show that the presence of $p$-GO induces conformational changes in HSA and malfunction in its binding capacity to bilirubin, leading to potential toxicity. Thus, the toxic effect of GO on plasma proteins must be looked into further. For the cytotoxic analysis of GO at high concentration, $p$-GO is found adsorbed on cell membrane without internalization or membrane disruption, but it induces a reduction in cell viability, increased intracellular ROS, moderate DNA damage, and T lymphocyte apoptosis. Interestingly, although $p$-GO induces an obvious decrease in cell viability and apoptosis, its influence on T lymphocytes immune response suppression is insignificant. GO-COOH shows a similar effect on T lymphocytes as $p$-GO except keeping normal intracellular ROS level. GO-PEI has a severe toxic effect on T lymphocytes with physical damage to the plasma membrane, grave DNA damage and suppression of T lymphocyte immune response ability. For plasma protein HSA, GO-COOH binds to HSA with minimum conformational and functional changes, whereas GO-PEI severely destroys the structure and function of HSA. So far, the doses of GO used are generally lower than 25 $\mu$g mL$^{-1}$ for drug delivery systems, cellular imaging and anticancer therapy applications. Our results indicate that GO-COOH in this range of concentration is a promising nanomaterial for biomedical applications. Through a

systematical cytotoxic analysis of GO at high concentration, a proposed toxic mechanism is that *p*-GO inhibits the binding of protein receptors with ligands and induces passive apoptosis depending on the increase in ROS. GO-COOH interacts with membrane protein receptor and passes the passive apoptosis signal to nucleus DNA through a ROS-independent mechanism. GO-PEI shows severe hematotoxicity to T lymphocytes by inducing membrane damage. We also conclude that positively charged particles are more toxic to cells than negatively charged particles, and carboxyl modification is an effective method to inhibit intracellular ROS generation. These findings are essential for the biomedical applications and safety assessment of GO.

## ■ ASSOCIATED CONTENT

### Supporting Information

UV−vis spectra, FT-IR spectra, zeta potential of GO, and additional experimental details. This material is available free of charge via the Internet at http://pubs.acs.org.

## ■ AUTHOR INFORMATION

### Corresponding Author

*E-mail: yychen2006@sinano.ac.cn. Tel: +86-512-62872596. Fax: +86-512-62872562.

### Notes

The authors declare no competing financial interest.

## ■ ACKNOWLEDGMENTS

The authors are thankful for the financial support by National Natural Science Foundation of China (11274345) and Chinese Academy of Sciences.

## ■ REFERENCES

(1) Geim, A. K. Graphene: Status and Prospects. *Science* **2009**, *324*, 1530−1534.
(2) Loh, K. P.; Bao, Q. L.; Eda, G.; Chhowalla, M. Graphene Oxide as a Chemically Tunable Platform for Optical Applications. *Nat. Chem.* **2010**, *2*, 1015−1024.
(3) Wang, Y.; Li, Z. H.; Wang, J.; Li, J. H.; Lin, Y. H. Graphene and Graphene Oxide: Biofunctionalization and Applications in Biotechnology. *Trends Biotechnol.* **2011**, *29*, 205−212.
(4) Singh, V.; Joung, D.; Zhai, L.; Das, S.; Khondaker, S. I.; Seal, S. Graphene based Materials: Past, Present and Future. *Prog. Mater. Sci.* **2011**, *56*, 1178−1271.
(5) Sun, X. M.; Liu, Z.; Welsher, K.; Robinson, J. T.; Goodwin, A.; Zaric, S.; Dai, H. J. Nano-Graphene Oxide for Cellular Imaging and Drug Delivery. *Nano Res.* **2008**, *1*, 203−212.
(6) Liu, Z.; Robinson, J. T.; Sun, X. M.; Dai, H. J. PEGylated Nanographene Oxide for Delivery of Water-Insoluble Cancer Drugs. *J. Am. Chem. Soc.* **2008**, *130*, 10876−10877.
(7) Yang, X. Y.; Zhang, X. Y.; Liu, Z. F.; Ma, Y. F.; Huang, Y.; Chen, Y. High-Efficiency Loading and Controlled Release of Doxorubicin Hydrochloride on Graphene Oxide. *J. Phys. Chem. C* **2008**, *112*, 17554−17558.
(8) Zhang, L. M.; Xia, J. G.; Zhao, Q. H.; Liu, L. W.; Zhang, Z. J. Functional Graphene Oxide as a Nanocarrier for Controlled Loading and Targeted Delivery of Mixed Anticancer Drugs. *Small* **2010**, *6*, 537−544.
(9) Ha, C. S.; Rana, V. K.; Choi, M. C.; Kong, J. Y.; Kim, G. Y.; Kim, M. J.; Kim, S. H.; Mishra, S.; Singh, R. P. Synthesis and Drug-Delivery Behavior of Chitosan-Functionalized Graphene Oxide Hybrid Nanosheets. *Macromol. Mater. Eng.* **2011**, *296*, 131−140.
(10) Dong, H. F.; Ding, L.; Yan, F.; Ji, H. X.; Ju, H. X. The Use of Polyethylenimine-Grafted Graphene Nanoribbon for Cellular Delivery of Locked Nucleic Acid Modified Molecular Beacon for Recognition of MicroRNA. *Biomaterials* **2011**, *32*, 3875−3882.
(11) Feng, L. Z.; Zhang, S. A.; Liu, Z. A. Graphene based Gene Transfection. *Nanoscale* **2011**, *3*, 1252−1257.
(12) Zhang, L. M.; Lu, Z. X.; Zhao, Q. H.; Huang, J.; Shen, H.; Zhang, Z. J. Enhanced Chemotherapy Efficacy by Sequential Delivery of siRNA and Anticancer Drugs Using PEI-Grafted Graphene Oxide. *Small* **2011**, *7*, 460−464.
(13) Bao, H. Q.; Pan, Y. Z.; Ping, Y.; Sahoo, N. G.; Wu, T. F.; Li, J.; Gan, L. H.; Li, L. Chitosan-Functionalized Graphene Oxide as a Nanocarrier for Drug and Gene Delivery. *Small* **2011**, *7*, 1569−1578.
(14) Yang, K.; Zhang, S. A.; Zhang, G. X.; Sun, X. M.; Lee, S. T.; Liu, Z. A. Graphene in Mice: Ultrahigh In Vivo Tumor Uptake and Efficient Photothermal Therapy. *Nano Lett.* **2010**, *10*, 3318−3323.
(15) Robinson, J. T.; Tabakman, S. M.; Liang, Y.; Wang, H.; Sanchez Casalongue, H.; Vinh, D.; Dai, H. Ultrasmall Reduced Graphene Oxide with High Near-Infrared Absorbance for Photothermal Therapy. *J. Am. Chem. Soc.* **2011**, *133*, 6825−6831.
(16) Tian, B.; Wang, C.; Zhang, S.; Feng, L.; Liu, Z. Photothermally Enhanced Photodynamic Therapy Delivered by Nano-Graphene Oxide. *ACS Nano* **2011**, *5*, 7000−7009.
(17) Yang, K.; Li, Y.; Tan, X.; Peng, R.; Liu, Z. Behavior and Toxicity of Graphene and its Functionalized Derivatives in Biological Systems. *Small* **2013**, *9*, 1492−1503.
(18) Bianco, A. Graphene: Safe or Toxic? The Two Faces of the Medal. *Angew. Chem., Int. Ed.* **2013**, *52*, 4986−4997.
(19) Seabra, A. B.; Paula, A. J.; de Lima, R.; Alves, O. L.; Duran, N. Nanotoxicity of Graphene and Graphene oxide. *Chem. Res. Toxicol.* **2014**, *27*, 159−168.
(20) Wang, K.; Ruan, J.; Song, H.; Zhang, J. L.; Wo, Y.; Guo, S. W.; Cui, D. X. Biocompatibility of Graphene Oxide. *Nanoscale Res. Lett.* **2011**, *6*, 8.
(21) Duch, M. C.; Budinger, G. R. S.; Liang, Y. T.; Soberanes, S.; Urich, D.; Chiarella, S. E.; Campochiaro, L. A.; Gonzalez, A.; Chandel, N. S.; Hersam, M. C.; Mutlu, G. M. Minimizing Oxidation and Stable Nanoscale Dispersion Improves the Biocompatibility of Graphene in the Lung. *Nano Lett.* **2011**, *11*, 5201−5207.
(22) Zhang, X. Y.; Yin, J. L.; Peng, C.; Hu, W. Q.; Zhu, Z. Y.; Li, W. X.; Fan, C. H.; Huang, Q. Distribution and Biocompatibility Studies of Graphene Oxide in Mice after Intravenous Administration. *Carbon* **2011**, *49*, 986−995.
(23) Vallabani, N. V. S.; Mittal, S.; Shukla, R. K.; Pandey, A. K.; Dhakate, S. R.; Pasricha, R.; Dhawan, A. Toxicity of Graphene in Normal Human Lung Cells (BEAS-2B). *J. Biomed. Nanotechnol.* **2011**, *7*, 106−107.
(24) Yuan, J. F.; Gao, H. C.; Ching, C. B. Comparative Protein Profile of Human Hepatoma HepG2 Cells Treated with Graphene and Single-Walled Carbon Nanotubes: An iTRAQ-Coupled 2D LC-MS/MS Proteome Analysis. *Toxicol. Lett.* **2011**, *207*, 213−221.
(25) Mullick Chowdhury, S.; Lalwani, G.; Zhang, K.; Yang, J. Y.; Neville, K.; Sitharaman, B. Cell Specific Cytotoxicity and Uptake of Graphene Nanoribbons. *Biomaterials* **2013**, *34*, 283−293.
(26) Yue, H.; Wei, W.; Yue, Z.; Wang, B.; Luo, N.; Gao, Y.; Ma, D.; Ma, G.; Su, Z. The Role of the Lateral Dimension of Graphene Oxide in the Regulation of Cellular Responses. *Biomaterials* **2012**, *33*, 4013−4021.
(27) Liao, K. H.; Lin, Y. S.; Macosko, C. W.; Haynes, C. L. Cytotoxicity of Graphene Oxide and Graphene in Human Erythrocytes and Skin Fibroblasts. *ACS Appl. Mater. Interfaces* **2011**, *3*, 2607−2615.
(28) Chang, Y. L.; Yang, S. T.; Liu, J. H.; Dong, E.; Wang, Y. W.; Cao, A. N.; Liu, Y. F.; Wang, H. F. In Vitro Toxicity Evaluation of Graphene Oxide on A549 Cells. *Toxicol. Lett.* **2011**, *200*, 201−210.
(29) Zhang, S. A.; Yang, K.; Feng, L. Z.; Liu, Z. In Vitro and in Vivo Behaviors of Dextran Functionalized Graphene. *Carbon* **2011**, *49*, 4040−4049.
(30) Sasidharan, A.; Panchakarla, L. S.; Sadanandan, A. R.; Ashokan, A.; Chandran, P.; Girish, C. M.; Menon, D.; Nair, S. V.; Rao, C. N.; Koyakutty, M. Hemocompatibility and Macrophage Response of Pristine and Functionalized Graphene. *Small* **2012**, *8*, 1251−63.
(31) Singh, S. K.; Singh, M. K.; Nayak, M. K.; Kumari, S.; Shrivastava, S.; Gracio, J. J. A.; Dash, D. Thrombus Inducing Property of Atomically Thin Graphene Oxide Sheets. *ACS Nano* **2011**, *5*, 4987−4996.

(32) Singh, S. K.; Singh, M. K.; Kulkarni, P. P.; Sonkar, V. K.; Grácio, J. J.; Dash, D. Amine-Modified Graphene: Thrombo-Protective Safer Alternative to Graphene Oxide for Biomedical Applications. *ACS Nano* **2012**, *6*, 2731−2740.
(33) Zhi, X.; Fang, H. L.; Bao, C. C.; Shen, G. X.; Zhang, J. L.; Wang, K.; Guo, S. W.; Wan, T.; Cui, D. X. The Immunotoxicity of Graphene Oxides and the Effect of PVP-Coating. *Biomaterials* **2013**, *34*, 5254−5261.
(34) Zolnik, B. S.; González-Fernández, Á.; Sadrieh, N.; Dobrovolskaia, M. A. Minireview: Nanoparticles and the Immune System. *Endocrinology* **2010**, *151*, 458−465.
(35) Tsoukas, C. D.; Landgraf, B.; Bentin, J.; Valentine, M.; Lotz, M.; Vaughan, J. H.; Carson, D. A. Activation of Resting T lymphocytes by Anti-CD3 (T3) Antibodies in the Absence of Monocytes. *J. Immunol.* **1985**, *135*, 1719−1723.
(36) Fehske, K. J.; Muller, W. E.; Wollert, U. The Location of Drug-Binding Sites in Human-Serum Albumin. *Biochem. Pharmacol.* **1981**, *30*, 687−692.
(37) Blauer, G.; Harmatz, D.; Naparste, A. Circular Dichroism of Bilirubin-Human Serum Albumin Complexes in Aqueous Solution. *FEBS Lett.* **1970**, *9*, 53−55.
(38) Hummers, W. S.; Offeman, R. E. Preparation of Graphitic Oxide. *J. Am. Chem. Soc.* **1958**, *80*, 1339−1339.
(39) Lai, Q.; Zhu, S.; Luo, X.; Zou, M.; Huang, S. Ultraviolet-Visible Spectroscopy of Graphene Oxides. *AIP Adv.* **2012**, *2*, 032146.
(40) Mu, Q.; Su, G.; Li, L.; Gilbertson, B. O.; Yu, L. H.; Zhang, Q.; Sun, Y.-P.; Yan, B. Size-Dependent Cell Uptake of Protein-Coated Graphene Oxide Nanosheets. *ACS Appl. Mater. Interfaces* **2012**, *4*, 2259−2266.
(41) Heiniger, H.-J.; Sodergren, A.; Marshall, J. D. Endocytosis in Cytotoxic T-Lymphocytes. *Cell Immunol.* **1981**, *59*, 429−434.
(42) Hu, W. B.; Peng, C.; Luo, W. J.; Lv, M.; Li, X. M.; Li, D.; Huang, Q.; Fan, C. H. Graphene-Based Antibacterial Paper. *ACS Nano* **2010**, *4*, 4317−4323.
(43) Akhavan, O.; Ghaderi, E. Toxicity of Graphene and Graphene Oxide Nanowalls Against Bacteria. *ACS Nano* **2010**, *4*, 5731−5736.
(44) Sanchez, V. C.; Jachak, A.; Hurt, R. H.; Kane, A. B. Biological Interactions of Graphene-Family Nanomaterials: an Interdisciplinary Review. *Chem. Res. Toxicol.* **2011**, *25*, 15−34.
(45) Agemy, L.; Sugahara, K. N.; Kotamraju, V. R.; Gujraty, K.; Girard, O. M.; Kono, Y.; Mattrey, R. F.; Park, J.-H.; Sailor, M. J.; Jimenez, A. I. Nanoparticle-Induced Vascular Blockade in Human Prostate Cancer. *Blood* **2010**, *116*, 2847−2856.
(46) Lenardo, M.; Chan, F. K.-M.; Hornung, F.; McFarland, H.; Siegel, R.; Wang, J.; Zheng, L. Mature T lymphocyte Apoptosis-Immune Regulation in a Dynamic and Unpredictable Antigenic Environment 1. *Annu. Rev. Immunol.* **1999**, *17*, 221−253.
(47) Strasser, A.; Harris, A.; Huang, D.; Krammer, P.; Cory, S. Bcl-2 and Fas/APO-1 Regulate Distinct Pathways to Lymphocyte Apoptosis. *EMBO J.* **1995**, *14*, 6136.
(48) Hockenbery, D. M.; Oltvai, Z. N.; Yin, X.-M.; Milliman, C. L.; Korsmeyer, S. J. Bcl-2 Functions in an Antioxidant Pathway to Prevent Apoptosis. *Cell* **1993**, *75*, 241−251.
(49) Kane, D. J.; Sarafian, T. A.; Anton, R.; Hahn, H.; Gralla, E. B.; Valentine, J. S.; Ord, T.; Bredesen, D. E. Bcl-2 Inhibition of Neural Death: Decreased Generation of Reactive Oxygen Species. *Science* **1993**, *262*, 1274−1277.
(50) Jacobson, M. D.; Raff, M. C. Programmed Cell Death and Bcl-2 Protection in Very Low Oxygen. *Nature* **1995**, *374*, 814−816.
(51) Jacobson, M. D. Reactive Oxygen Species and Programmed Cell Death. *Trends Biochem. Sci.* **1996**, *21*, 83−86.
(52) Budinger, G. S.; Tso, M.; McClintock, D. S.; Dean, D. A.; Sznajder, J. I.; Chandel, N. S. Hyperoxia-Induced Apoptosis Does Not Require Mitochondrial Reactive Oxygen Species and Is Regulated by Bcl-2 Proteins. *J. Biol. Chem.* **2002**, *277*, 15654−15660.
(53) Distelhorst, C. W.; Shore, G. C. Bcl-2 and Calcium: Controversy beneath the Surface. *Oncogene* **2004**, *23*, 2875−2880.
(54) Antonsson, B.; Conti, F.; Ciavatta, A.; Montessuit, S.; Lewis, S.; Martinou, I.; Bernasconi, L.; Bernard, A.; Mermod, J.-J.; Mazzei, G. Inhibition of Bax Channel-Forming Activity by Bcl-2. *Science* **1997**, *277*, 370−372.
(55) Penhale, W.; Farmer, A.; Maccuish, A.; Irvine, W. A Rapid Micro-Method for the Phytohaemagglutinin-Induced Human Lymphocyte Transformation Test. *Clin. Exp. Immunol.* **1974**, *18*, 155.
(56) Hu, W. B.; Peng, C.; Lv, M.; Li, X. M.; Zhang, Y. J.; Chen, N.; Fan, C. H.; Huang, Q. Protein Corona-Mediated Mitigation of Cytotoxicity of Graphene Oxide. *ACS Nano* **2011**, *5*, 3693−3700.
(57) Shen, M.; Wang, S. H.; Shi, X.; Chen, X.; Huang, Q.; Petersen, E. J.; Pinto, R. A.; Baker, J. R., Jr; Weber, W. J., Jr Polyethyleneimine-Mediated Functionalization of Multiwalled Carbon Nanotubes: Synthesis, Characterization, and In Vitro Toxicity Assay. *J. Phys. Chem. C* **2009**, *113*, 31.
(58) Bhattacharjee, S.; de Haan, L. H.; Evers, N. M.; Jiang, X.; Marcelis, A. T.; Zuilhof, H.; Rietjens, I. M.; Alink, G. M. Role of Surface Charge and Oxidative Stress in Cytotoxicity of Organic Monolayer-Coated Silicon Nanoparticles towards Macrophage NR8383 Cells. *Part. Fibre Toxicol.* **2010**, *7*, 25−36.
(59) Li, L. W.; Mu, Q. X.; Zhang, B.; Yan, B. Analytical Strategies for Detecting Nanoparticle-Protein Interactions. *Analyst* **2010**, *135*, 1519−1530.
(60) Lacerda, S. H. D.; Park, J. J.; Meuse, C.; Pristinski, D.; Becker, M. L.; Karim, A.; Douglas, J. F. Interaction of Gold Nanoparticles with Common Human Blood Proteins. *ACS Nano* **2010**, *4*, 365−379.